CHAPTER 4

Stabilization of CeO_2/BC with pre-treated biochar for nitrate removal

4.1 INTRODUCTION

The United Nations has identified safe drinking water as a critical global challenge. Goal 6 of the Sustainable Development Goals specifically targets this issue, emphasizing the need to ensure access to clean water for all. The severity of the problem is underscored by the fact that approximately one-third of the world's population currently lacks access to safe drinking water [91]. Nitrate is a prevalent environmental contaminant that poses a global health risk due to its presence in both food and drinking water. Countries with intensive agricultural practices, such as the United States, China, and those in Europe, are particularly susceptible to nitrate leaching into groundwater supplies [217]. Nitrate levels in groundwater have shown a declining trend across many European countries. However, significant challenges persist as numerous nations are still unable to fully comply with the stringent standards outlined in the EU's Groundwater and Drinking Water Directives [218,219]. Conversely, developing countries are experiencing escalating nitrate contamination. This trend is closely linked to increased nitrogen fertilizer use and rapid economic growth in these regions [91,220,221]. Consumption of nitrate-contaminated drinking water has been associated with an increased risk of various cancers, including colorectal, stomach, ovarian, thyroid, kidney, and bladder cancers (Inoue-Choi et al., 2015; Temkin et al., 2019; Ward et al., 2018). Ward et al identified colorectal cancer, thyroid disease, and neural tube defects as the health conditions with the strongest indication of a link to nitrate ingestion from drinking water, excluding methemoglobinemia [222]. Furthermore, the International Agency for Research on Cancer (IARC) has classified ingested nitrate and nitrite, which can form nitrosamines, as possibly carcinogenic to humans, placing them in Group 2A (Picetti et al., 2022). Moreover, elevated nitrate concentrations in water bodies can lead to detrimental ecological impacts such as eutrophication, fish mortality, and harmful algal blooms (Liu & Wang, 2019). Removing nitrate from drinking water remains a significant challenge due to its high solubility and stability in aquatic environments. Several treatment

technologies have been used to remove nitrate from water including reverse osmosis [224], ion exchange [225], electrochemical reduction [226], catalytic reduction [227], biological denitrification [228], and adsorption [229]. Of the aforementioned techniques, adsorption is considered the most promising approach for nitrate removal due to its operational simplicity, straightforward design, and low associated costs [229]. To achieve effective nitrate removal through adsorption, the adsorbent material must possess a high capacity for nitrate uptake, exhibit strong resistance to chemical degradation, and be easily regenerated for repeated use.

Formed under oxygen-limited conditions through the pyrolysis of biomass, biochar, a carbonaceous material, has been identified as a promising adsorbent for nitrate removal. A variety of biomass feedstocks, including elephant grass [230], corncob [231], wheat-straw [232] were used as precursors to prepare biochar for nitrate removal. Biochar is characterized by desirable properties including high cation exchange capacity, carbon stability, water retention capacity, and porosity. To further enhance these attributes, metal-based compounds like $FeCl_3$ and MgFe-LDH, are often used to improve the properties of biochar [232–234]. Research indicates that metal modification significantly enhances biochar's ability to retain metal ions through the formation of metal oxides [233].

Sugarcane bagasse was selected for biochar synthesis for a variety of reasons. It is a major agricultural waste product generated by the sugarcane industry, especially in countries such as Brazil, Mexico, and China [235,236]. Its large output has resulted in significant environmental pressure, making it an ideal candidate for resource utilization. Sugarcane bagasse is composed primarily of lignin, cellulose, and hemicellulose, which renders it a particularly suitable feedstock for biochar synthesis. These components give sugarcane bagasse biochar a porous structure and abundant oxygen-containing functional groups, which enhance its ability to adsorb organic and inorganic pollutants [237]. Researchers can promote better waste

management and reduce environmental pollution by transforming sugarcane bagasse into biochar. This sustainable method is in line with principles of resource efficiency and environmental conservation.

This study utilizes a novel adsorbent, cerium-impregnated biochar, for the first time to remove nitrate from drinking water. Previous research has demonstrated its exceptional ability to remove fluoride from drinking water. As a result, it is anticipated that this adsorbent will effectively address nitrate pollution and safeguard human health.

4.2. METHODOLOGY AND EXPERIMENTAL

4.2.1 Pre- Treatment of Raw biochar

Before stabilizing it with cerium, the unmodified biochar underwent oxidation, acid, and base treatments. The oxidation modification of biochar involved soaking the raw biochar in a 30% H_2O_2 solution at ambient temperature for 24 hours (using a 1:100 solid-solution ratio) [238]. Subsequently, the sample was washed with deionized water multiple times before being dried at 80°C for 8 hours. The base and acid treatments of the biochar were conducted by immersing it in either a 1 M KOH or a 1 M HCl solution for 24 hours. The samples were then treated following the same steps as the oxidation modification, resulting in base-modified biochar and acid-modified biochar [239]. Plain biochar as obtained was named as SB.

4.2.2 Stabilization of Cerium oxide on pre-treated biochar

Cerium supported biochar composite samples were prepared through the procedure described elsewhere [240]. Ammonium cerium nitrate was dissolved in de-ionized water and stirred for 60 minutes at 40°C. Simultaneously, the necessary amount of modified or treated biochar was stirred in another beaker for 60 minutes at 40°C. Subsequently, both solutions were combined and kept stirring at 60°C. Ammonium hydroxide solution was slowly added to the stirring

mixture until the pH reached 12. The solution was left overnight to promote the precipitate's development. The solid was then filtered, rinsed multiple times with deionized water, and washed with ethanol. Next, the resulting material underwent heating in a hot air oven at 80°C for 12 hours. The untreated biochar was also modified using the same method. These samples were labeled as HCB (treated with H_2O_2), KBC (treated with KOH), HCLB (treated with HCl), and CeO_2/BC (untreated biochar).

4.2.3 Characterization of adsorbents

The synthesis of adsorbents and its physical as well as chemical properties were characterized with different characterization tools such as SEM, BET, XRD, FTIR, and pHzpc measurement.

4.2.4 Nitrate batch adsorption experiments

Nitrate removal by four different types of synthesized composites HCB, KBC, HCLB, CeO_2/BC and SB. All these were examined by adding the composites (200 mg/L) into 25 mL Nitrate solution (20 mg/L) at room temperature (25 ± 2 ˚C). After that, the capped Erlenmeyer flask was shaken at 200 rpm immediately. Then the samples were withdrawn and centrifuged at selected time intervals for the analysis of nitrate by Metrohm Dual Channel 930 Compact IC Flex. The effects of solution pH, contact time and initial nitrate concentration on its removal were also examined. The effect of pH was studied by adjusting initial pH from 2 to 10 using 0.1 M HCl or 0.1 M NaOH in a condition of 20 mg/L nitrate concentration and 200 mg/L composites. The effect of initial nitrate concentration on its removal was carried out by varying the concentration from 10 to 90 mg/L in the presence of 200 mg/L composites. At defined time intervals, the suspension was filtered using 0.45 m membranes, and the concentration of residual nitrate in the filtrate was determined. Adsorption kinetics experiments were executed with a dose of 200 mg/L, an initial solution pH value of 7±1, and 20 mg/L of nitrate

concentration kept for shaking for 360 min. Then the samples were collected by filtration and residual concentration was calculated. Adsorption isotherm experiments were run at various initial nitrate concentrations (10–90 mg/L), a dosage of 200 mg/L, and an initial pH value of 7±1 for 360 min. Then the samples were collected by filtration and residual concentration was calculated.

4.3. BIOCHAR SAMPLE CHARACTERISATION

4.3.1 XRD analysis

The XRD pattern of the HBB (HB before adsorption) exhibited a broad peak ranging from 2θ (20° to 30°) (Fig. 4.1) characteristic of an amorphous carbon diffraction pattern, and corresponded with findings in existing literature [241,242]. In contrast to the HBB biochar, the XRD pattern of the cerium-modified biochar HCBB (HCB before adsorption) revealed sharp and well-defined peaks (Fig. 4.1). These peaks were successfully indexed to the crystalline structure of face centered cubic cerium oxide (CeO_2) using JCPDS File No. 34-0394. The presence of distinct peaks at 2θ 28.53°, 33.0°, 47.5°, and 56.26° corresponds to the miller indices (111), (200), (220), and (311) of CeO_2, respectively. This observation confirms the successful incorporation of crystalline CeO_2 onto the biochar matrix.

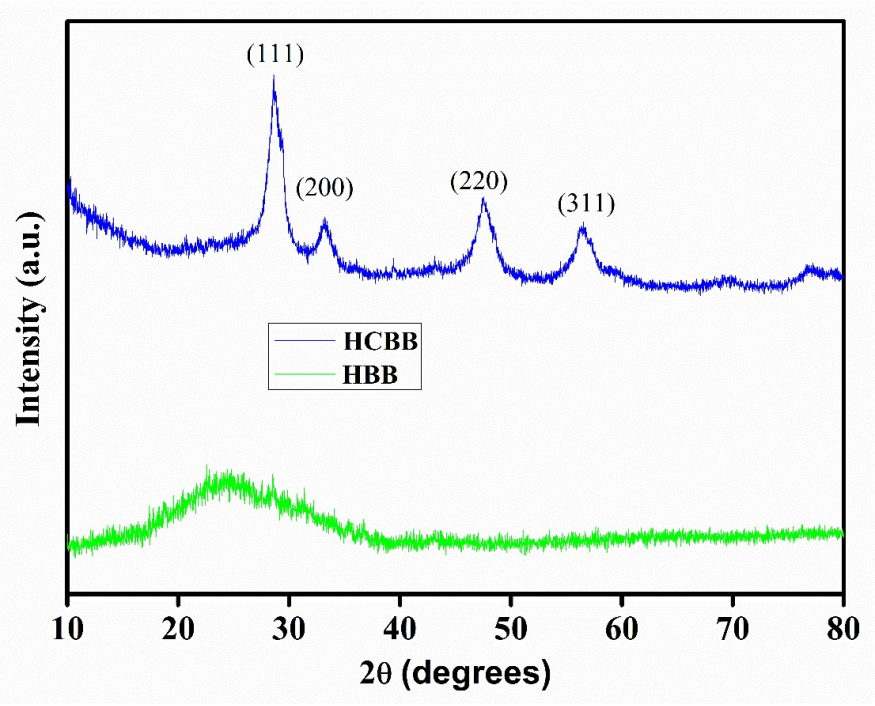

Figure. 4.1 XRD diffractograms of sugarcane biochar (HBB) and CeO_2/BC (HCBB)

4.3.2 BET analysis

BET Surface area analysis of HBB and HCBB biochar reveals that both materials display type IV isotherms with H2 hysteresis loops, indicating mesoporous properties (Fig. 4.2). The specific surface area of H_2O_2 modified raw biochar (HBB) was found to be 151.49 m^2/g, with a pore volume of 0.12 cm^3/g and an average pore diameter of 3.1 nm. Upon modification of HBB with Cerium, a reduction in surface area to 131.23 m^2/g was observed, attributed to the incorporation of Cerium within the pores as can also be seen by SEM images. Furthermore, there was a slight increase in pore diameter to 3.32 nm in the modified biochar HCBB, which may have resulted in the development of new pores or interconnected previously isolated ones as a result of chemical precipitation or thermal treatment during modification process. The pore volume for the HCBB biochar was measured at 0.1 cm^3/g and nm, respectively. All the values are represented in the Table 4.1.

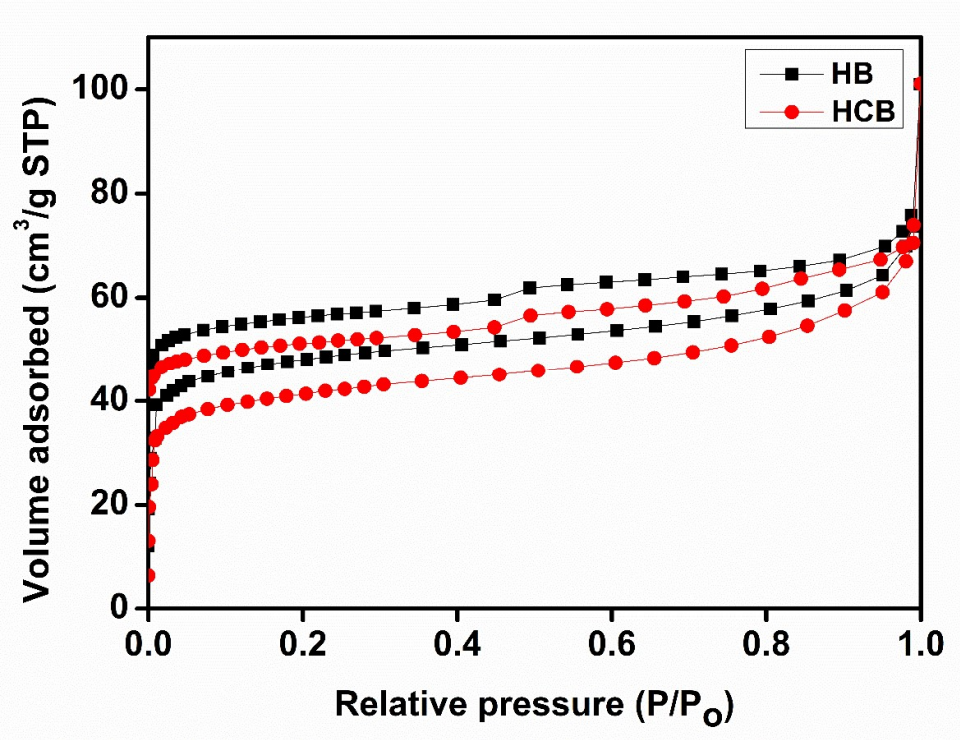

Figure 4.2 N_2 adsorption-desorption isotherms of H_2O_2 treated biochar's

Table 4.1 Comparing values of surface area, pore volume and pore size of synthesized raw biochar, and modified biochar HCBB

Sample description	BET surface area (m^2/g)	BJH average pore size (nm)	BJH pore volume (cm^3/g)
HBB	151.49	3.1	0.12
HCBB	131.23	3.32	0.1

4.3.3 FTIR analysis

The Fourier transform infrared spectroscopy analysis was conducted to examine the functional groups present in HBB, HCBB and HCBA (HCB after adsorption) biochar's (Fig. 4.3). Peaks at 3408 cm^{-1} in HBB, HCBB and HCBA were assigned to -OH stretching and vibration of

hydroxyl groups, indicating the presence of hydroxyl groups on the surface of the adsorbent. The symmetric and asymmetric C-H stretching vibrations between 2800 and 2900 cm^{-1} are due to aliphatic groups in biochar's. The C-C stretching vibration at 1565 cm^{-1} is of aromatic rings of lignin and the CO stretching vibration at 1063 cm^{-1} is of conjugated quinone and ketone. A decrease in peak density of -OH and Ce-O peak at 876 cm^{-1} after adsorption of nitrate in HCBA suggested the involvement of hydroxyl groups and Cerium in the adsorption process. New peaks appeared at 1384 cm^{-1} on the HCBA after adsorption, corresponding to the vibration of N-H group, indicating interactions between the adsorbent and nitrate during the adsorption process. Bands at 471 cm^{-1} and 876 cm^{-1} were associated with the stretching vibration of M-O, and M-OH (M=Ce), respectively, suggesting the involvement of these groups in the adsorption process. The intensity of 471 cm^{-1} and 876 cm^{-1} peaks was found to be higher in the cerium-modified biochar (HCBB and HCBA), indicating that the successful incorporation of cerium onto the biochar matrix.

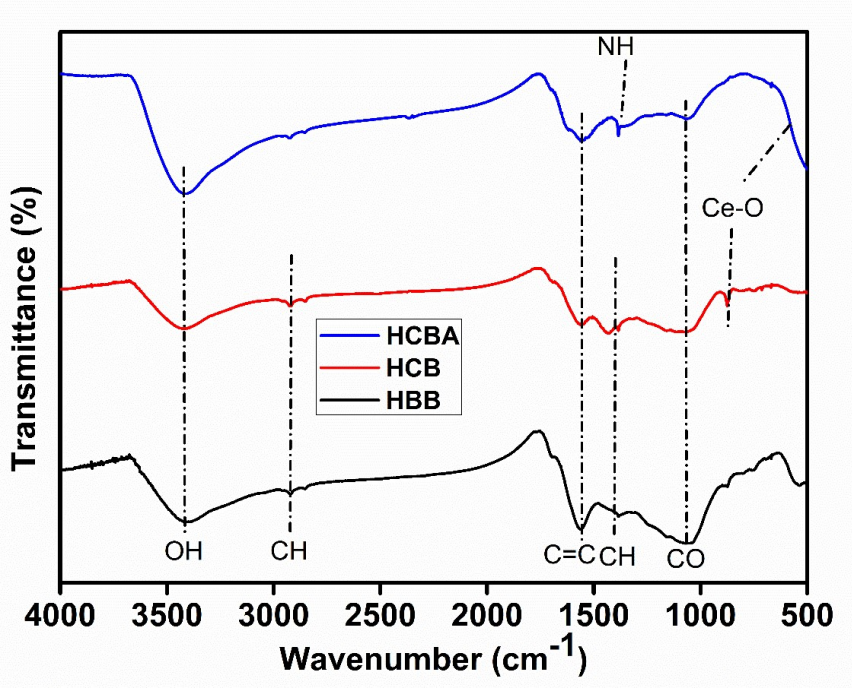

Figure 4.3 FTIR spectrum of H_2O_2 treated biochar before (HBB and HCB) and after adsorption (HCBA)

4.3.4 SEM analysis

From scanning electron microscope images, it is evident that the thermal decomposition of biomass resulted in the formation of fissures on the surface of the untreated biochar (Fig. 4.4). This development was caused by the liberation of volatile organic substances during the degradation of lignocellulosic matrix constituents. After treating the as-synthesized biochar with H_2O_2 (HB), noticeable alterations in its structure become evident. The pores appear more open and adopt a structured form, similar to a honeycomb (Fig. 4.4). After adding cerium to HB biochar through precipitation, we noticed the formation of small, irregularly shaped particles on its surface. The presence of cerium in HB was also evident from the filling of pores in the biochar by cerium (as illustrated in Fig. 4.4). This physical bonding resulting from the incorporation of cerium may contribute to the observed reduction in surface area of HCB as confirmed by the findings from BET analysis.

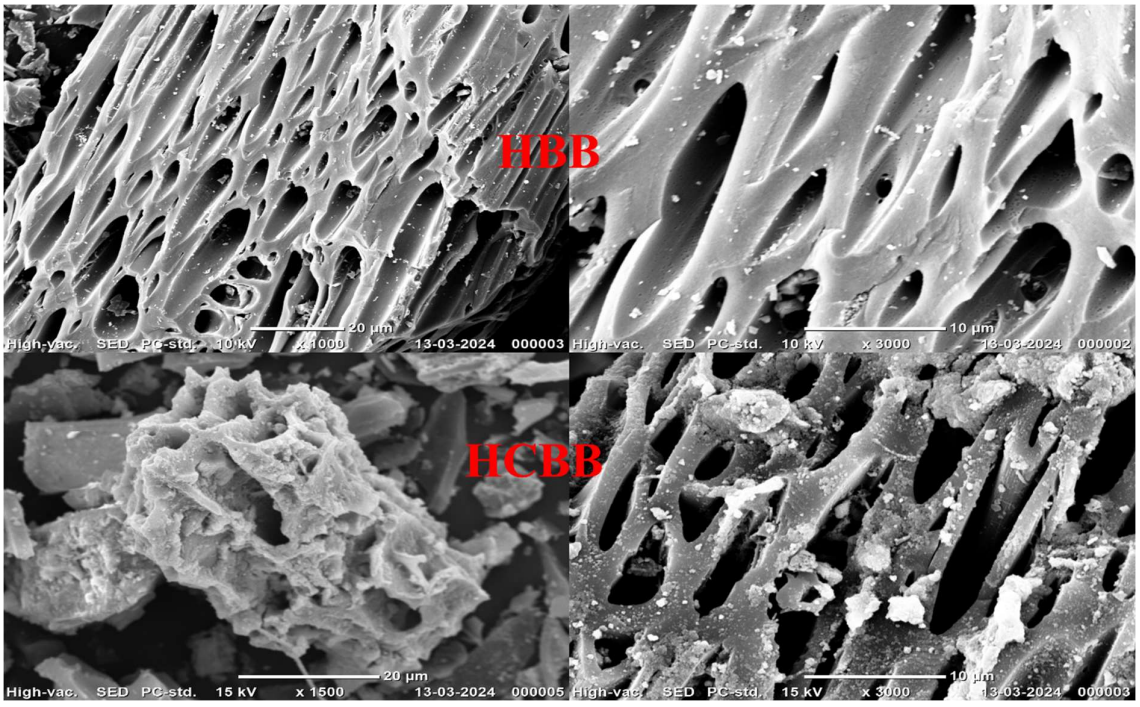

Figure 4.4 SEM images of H_2O_2 treated biochar's before adsorption

4.3.5 Surface charge / Zeta potential measurement

The surface charge characteristics of the HBB and HCBB biochars were evaluated using zeta potential measurements (Fig. 4.5). This technique provides valuable insights into the electrostatic interactions between the biochar surface and contaminants in aqueous environments [243]. Our results indicated that unmodified HBB possessed a negative surface charge across the entire pH range (2-10). This inherent negative charge is attributed to the ionization of carboxylic and phenolic functional groups present on the biochar surface [244]. As the pH increases, the deprotonation of these functional groups leads to a more negative surface charge due to the increased number of negatively charged sites (COO^- and O^-). This observation aligns with previous studies reporting a similar trend for various biochars [245].

In contrast, cerium-modified HCBB exhibited a pH-dependent surface charge behavior. At lower pH values (up to pH 5), the zeta potential measurements revealed a positive surface charge. This phenomenon can be attributed to the protonation of surface hydroxyl groups on the biochar and cerium oxide nanoparticles. Protons (H^+) can interact with these surface groups to form positively charged species (Ce-OH^{2+}). When the solution pH is below the point of zero charge (pHpzc) of HCBB (around pH 5.4), the net surface charge becomes positive due to the dominance of these protonated sites [246]. However, as the pH increases beyond pH 5, deprotonation of the surface functional groups becomes more favorable (Fig. 4.5). This leads to the gradual decrease in positive charge density and eventually results in a negatively charged surface at higher pH values (pH 6-10). This shift in surface charge from positive to negative with increasing pH is consistent with the reported behavior of other cerium-modified adsorbents [247].

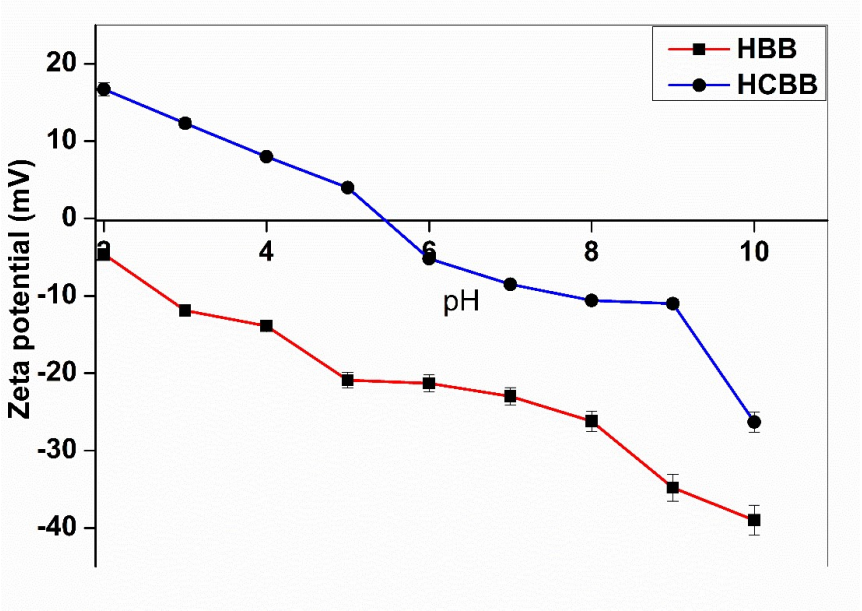

Figure 4.5 Zeta potential study of H_2O_2 treated biochar's before adsorption

4.4 BATCH ADSORPTION STUDIES

4.4.1 Nitrate removal by Cerium supported on modified biochars

This study investigated the impact of biochar modification on (NO_3^-) removal efficiency. Various biochar forms were employed, including raw biochar (SB), cerium oxide modified biochar without pretreatment (CeO_2/BC), and three pretreated cerium modified biochars (KCB, HCB, and HCLB). The results demonstrated a significant influence of modification methods on NO_3^- removal (Fig. 4.6). HCB exhibited the highest removal efficiency (72%), followed by HCLB and KCB (both at ~50%), while CeO_2/BC and SB displayed considerably lower removal rates (50% and 10%, respectively).

The low NO_3^- removal by raw biochar can be attributed to its negatively charged surface, as shown in the zeta potential data (Fig. 4.5). This negative charge creates a strong electrostatic repulsion against NO_3^-. Therefore, it is suggested that the biochar itself minimally contributes to NO_3^- removal in these composites.

For HCB superior performance compared to other modified biochars, several factors likely play a role. Biochar acts as a support for CeO_2 particles. The high surface area of biochar facilitates the even distribution of cerium ions on HCB, maximizing the contact area between the composite and NO_3^-. Additionally, this increased surface area provides more sites for precipitate deposition. The generated Ce-NO_3^- complexes during the reaction can be adsorbed onto the biochar surface through complexation with oxygen-containing functional groups, as confirmed by FTIR analysis (Fig. 4.3). Due to the superior NO_3^- removal observed with HCB, subsequent experiments in this study solely employed this modified biochar.

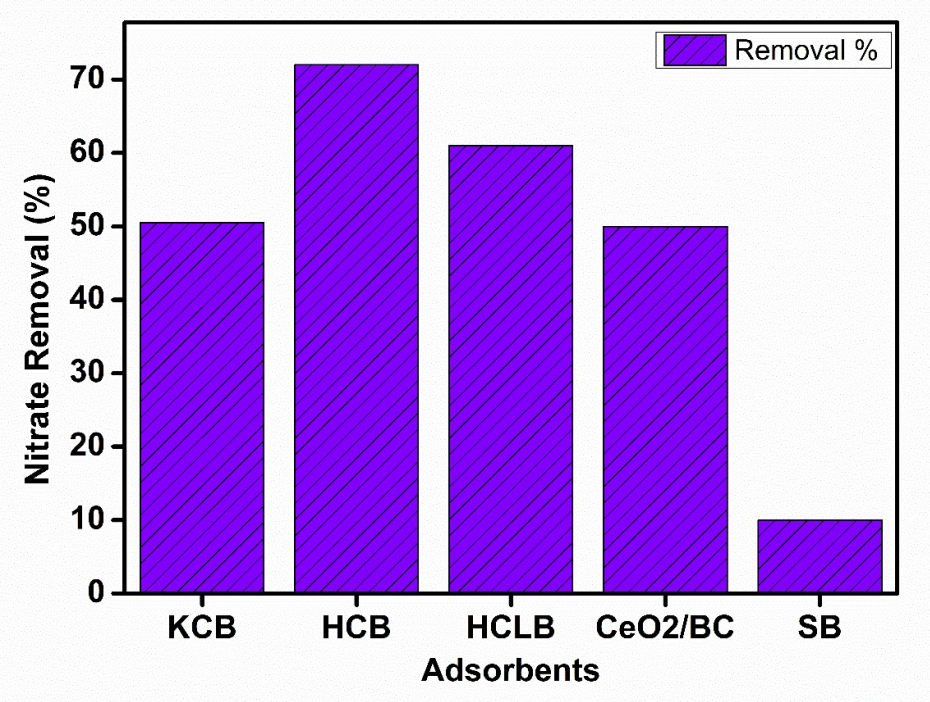

Figure 4.6 Effect of different activating agents of biochar on nitrate removal

4.4.2 Effect of initial pH on Nitrate removal

The adsorption of nitrate (NO_3^-) onto biochar's exhibited a strong dependence on the solution pH, with HCB (H_2O_2-pretreated biochar with cerium) demonstrating significantly higher

removal efficiency compared to unmodified HB (H_2O_2-pretreated biochar) across the entire pH range (2-10) (Fig. 4.7). This enhanced performance of HCB can be attributed to its higher surface positive charge density relative to HB, as confirmed by zeta potential measurements (Fig. 5.4). The solution pH plays a crucial role in governing the surface charge of the adsorbent, which in turn influences the electrostatic interactions with the target contaminant (NO_3^-) [248]. As observed in Fig. 4.5, both HCB and HB exhibited a decrease in zeta potential with increasing pH, indicating a gradual shift towards a more negative surface charge. However, a key distinction lies in the behaviour at lower pH values. HCB maintained a positive surface charge up to pH 5, whereas HB remained negatively charged throughout the investigated pH range. This observation aligns well with the superior NO_3^- removal by HCB at acidic pH (pH 2-5). In an acidic environment, the electrostatic attraction between the positively charged HCB surface and the negatively charged NO_3^- species is more favourable, leading to enhanced adsorption. This phenomenon is further supported by the maximum NO_3^- removal (76%) observed for HCB at pH 5. After pH 5 HCB surface became negatively charged increasing electrostatic repulsion hence decreasing removal of NO_3^-. In contrast, HB displayed a much lower and relatively constant NO_3^- removal efficiency (around 38%) across all pH values due to the absence of significant electrostatic attraction or the presence of repulsive forces between its negatively charged surface and NO_3^- ions.

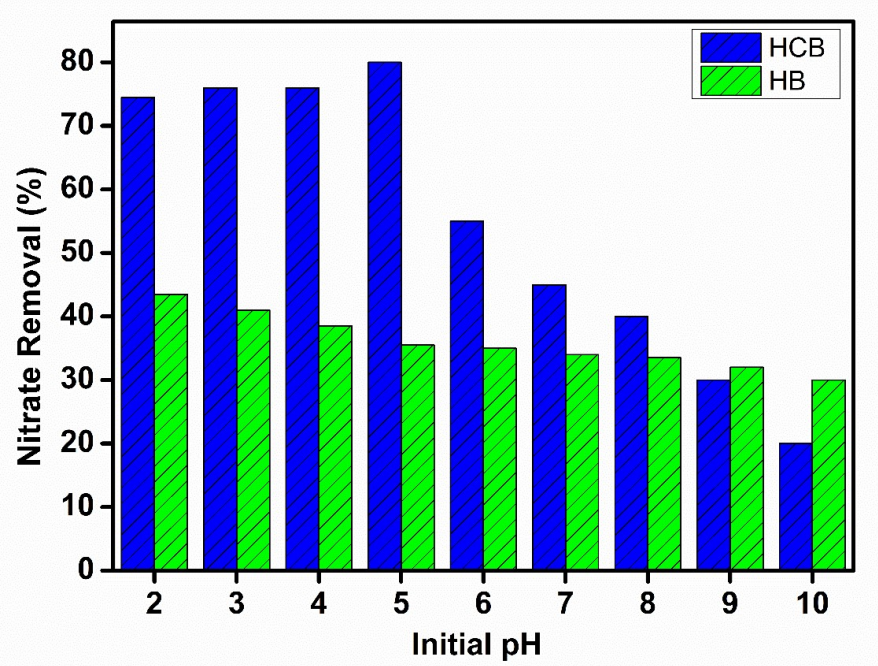

Figure 4.7 Effect of initial pH on nitrate removal

4.4.3 Effect of contact time on adsorption and kinetic studies

Figure 4.8 a illustrates the influence of contact time on the adsorption capacity of HCB and HB for nitrate removal. The data reveal a superior performance of HCB compared to HB. HCB exhibits a rapid initial uptake, achieving 72% nitrate removal within 60 minutes, significantly exceeding HB's performance (35% removal). HCB reaches equilibrium at 360 minutes, removing a total of 78% of nitrate. On the contrary, HB reaches equilibrium much faster (120 minutes) but with a lower removal efficiency (36%).

This disparity in removal kinetics can be attributed to the differing availability of active adsorption sites. HCB likely possesses a greater number of initially accessible sites, facilitating the swift initial uptake of nitrate. As the adsorption process progresses, these sites become occupied, leading to a gradual decrease in the adsorption rate until equilibrium is established when all active sites are saturated.

To elucidate the rate-limiting steps governing the adsorption process, the experimental data were fitted to both pseudo-first-order and pseudo- second-order kinetic models (explanation of models and mathematical equation given in chapter 2 section 2.5.2), (Fig. 4.8 b) (Table 4.2). The data exhibited a significantly better fit to the pseudo-second-order model, evidenced by a high correlation coefficient (R^2 = 0.99) and close agreement between the equilibrium adsorption capacity (q_e) predicted by the model and the experimentally observed value. This suggests that chemisorption, involving mechanisms like complex formation, electron sharing, or ion exchange, plays a dominant role in nitrate removal by HCB.

However, the high R^2 value obtained for the pseudo-first-order model also indicates the potential contribution of physical adsorption mechanisms. Electrostatic attraction between the negatively charged nitrate ions and the positively charged biochar surface could be a contributing factor.

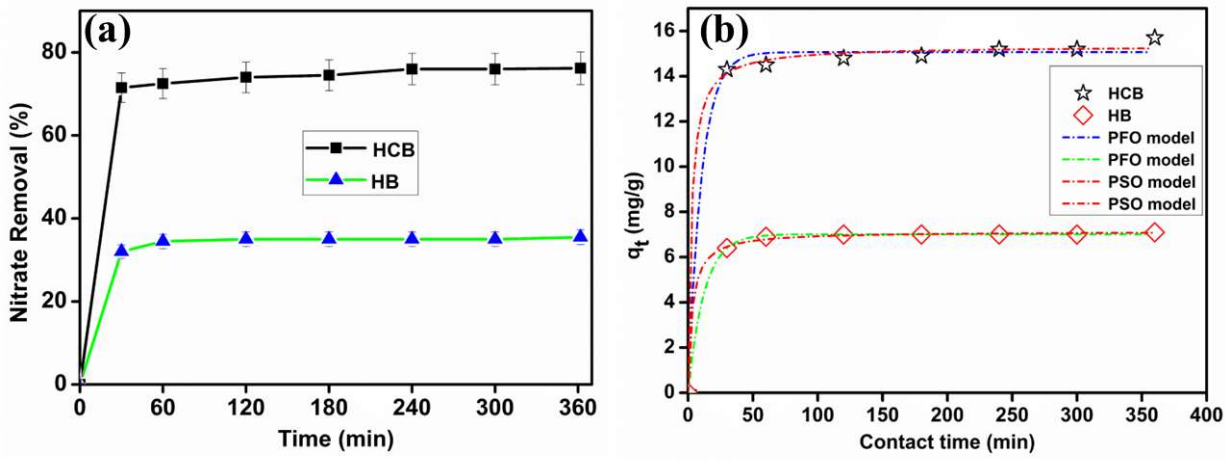

Figure 4.8 Effect of contact time (a); Plots of kinetic models of adsorption (b)

Table 4.2 Different kinetic models' parameter for nitrate uptake by H_2O_2 treated biochar's

Adsorbents	C_o (mg/L)	$q_{e(exp)}$ (mg/g)	Pseudo first order			Pseudo second order		
			qe (mg/g)	k_1 (min^{-1})	R^2	qe (mg/g)	k_2 (min^{-1})	R^2
HBB	20	7	7.01	0.08	0.99	7.14	0.04	0.99
HCB	20	15.2	15.06	0.09	0.99	15.33	0.025	0.99

4.4.4 Effect of Initial Nitrate Concentration and Mechanistic Insights

The effect of initial nitrate concentration on the adsorption capacity of HCB and HB biochar's was investigated using a concentration range of 10-90 mg/L (Fig. 4.9 a). The observed increase in nitrate uptake with increasing initial concentration is indicative of a concentration-driven adsorption process. This phenomenon can be attributed to the enhanced mass transfer between the solution and the composite due to the higher abundance of nitrate ions at elevated initial concentrations. This ultimately leads to greater interaction between the nitrate ions and the available adsorption sites on the composite surface.

To gain further insights into the underlying adsorption mechanism, the experimental data were fitted to both the Freundlich and Langmuir isotherm models (explanation of models and mathematical equation given in chapter 2 section 2.5.3). The Langmuir model exhibited a significantly superior fit, as evidenced by a high correlation coefficient (Fig. 4.9 b) (Table 4.3). This suggests a homogenous adsorption process where nitrate ions preferentially bind to specific, energetically favourable sites on the HCB and HB surface. The Langmuir isotherm calculates theoretical maximum adsorption capacity to be 15.2 mg/g for HCB and 7.5 mg/g for HB. In contrast, the Freundlich model, with its lower correlation coefficient, implies a more heterogeneous surface with a wider distribution of adsorption energies.

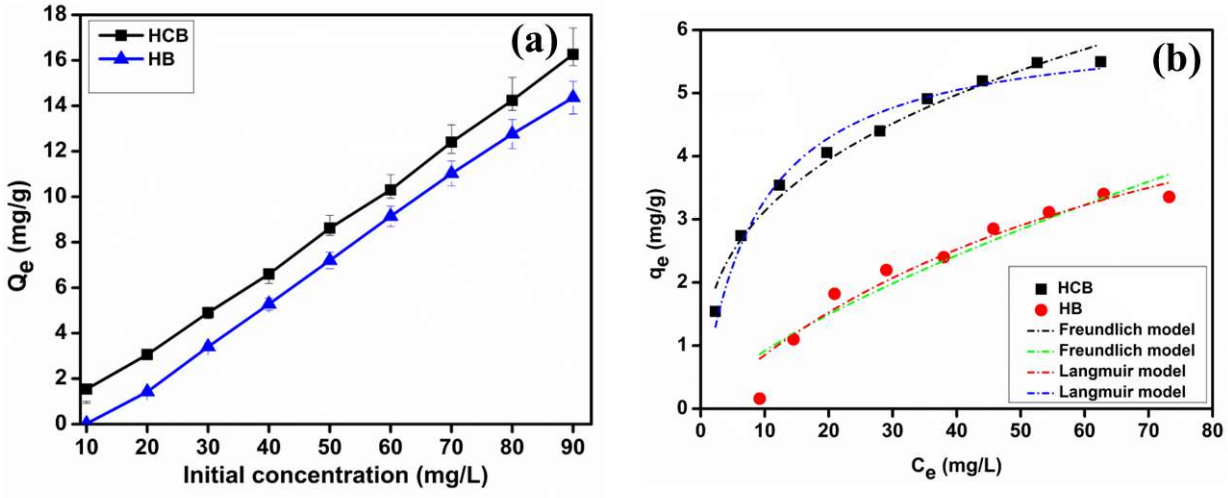

Figure 4.9 Effect of initial concentration (a); Plots of isotherm models of adsorption (b)

Table 4.3: Different isotherm models' parameter for nitrate uptake by H_2O_2 treated biochar's

Isotherm models	Parameters	HCB	HB
Langmuir Isotherm	**Q_m (mg/g)**	15.2	7.25
	k	0.11	0.01
	R^2	0.98	0.93
Freundlich Isotherm	**K_F (mg/g)**	1.45	0.18
	n	2.99	1.42
	R^2	0.97	0.90

4.5 CONCLUSIONS

This study successfully demonstrated the potential of cerium-impregnated biochar, particularly HCB (H_2O_2-pretreated biochar impregnated with cerium), as an effective adsorbent for nitrate removal from water. The characterization studies revealed that cerium modification enhanced the biochar's surface area and introduced new functional groups, contributing to improved adsorption capacity.

The results indicate that HCB exhibited superior nitrate removal efficiency (78% under optimal conditions) compared to unmodified biochar and other modified versions. The adsorption process was significantly influenced by pH, with optimal performance observed at pH 5. Kinetic studies suggested that chemisorption was the dominant mechanism, although physical adsorption also contributed to the overall process. The adsorption isotherm data were best fitted by the Langmuir model, suggesting a homogeneous adsorption process with specific binding sites on the HCB surface.

This research highlights the potential of utilizing agricultural waste-derived biochar as a sustainable and cost-effective adsorbent for nitrate removal. Further optimization of the modification process and exploration of other metal impregnations could lead to even greater removal efficiencies and broader applicability.